Journal of Catalysis **204,** 175–191 (2001)
doi:10.1006/jcat.2001.3370, available online at http://www.idealibrary.com on IDEAL®

NO_x Storage Reduction over Pt–Ba/γ-Al_2O_3 Catalyst

Luca Lietti, Pio Forzatti,[1] Isabella Nova, and Enrico Tronconi

Dipartimento di Chimica Industriale e Ingegneria Chimica "Giulio Natta" del Politecnico, Piazza Leonardo da Vinci 32, 20133 Milano, Italy

Received May 8, 2001; revised August 3, 2001; accepted August 4, 2001

A transient study on the NO_x storage-reduction properties of a Pt–BaO/γ-Al_2O_3 catalyst is performed by using a synthetic exhaust gas containing oxygen and nitrogen oxides (storage phase) and a reducing gas containing hydrogen (reduction phase). The influence of water and carbon dioxide is also investigated. It is found that (i) NO_x is stored in the form of nitrites and nitrates; (ii) during storage nitrites are oxidized to nitrates, and nitrates are most abundant when the storage process is completed; (iii) 0.3–3% CO_2 has a marked inhibiting effect on the storage of NO_x, particularly at low temperature, whereas 1% H_2O has a promoting effect at low temperature and an inhibiting effect at high temperature. In the presence of 0.3–3% CO_2 + 1% H_2O the process is inhibited at any temperature; (iv) the storage of NO_x occurs preferentially in the order at BaO, $Ba(OH)_2$, and $BaCO_3$. The abundance of the different Ba sites at the catalyst surface depends on the composition of the exhaust gas and of the reducing gas; (v) considerable amounts of NO_x are stored up to catalyst saturation and up to the NO_x breakthrough in He + 3% O_2 atmosphere that correspond to 24% Ba and 13–15% Ba to the best, respectively; (vi) in the presence of 0.3–3% CO_2 and 1% H_2O in the exhaust these quantities diminish by 20–40% for NO_x stored up to catalyst saturation and by 50% for NO_x stored up to the NO_x breakthrough; (vii) the reduction of the stored NO_x is fast and is limited by the concentration of the reducing agent at any temperature in He + 2000 ppm H_2; (viii) the reduction of the stored NO_x is very selective to N_2 (95–100%); (ix) the reduction is slower in the presence of 0.3–3% CO_2 and 0.3–3% CO_2 + 1% H_2O; (x) once all the stored reactive NO_x groups have been reduced, in the presence of 0.3–3% CO_2 and at sufficiently high temperature ($T \geq 300^\circ$C) CO is formed through the reverse WGS reaction. This reaction, however, is of lesser importance when water is present in the exhaust due to thermodynamic constraints. The complete set of reactions involved in the storage-reduction cycle is identified and used to account quantitatively for the bulk of experimental data and to provide a comprehensive chemistry of the process.

INTRODUCTION

Lean burn combustion is effective for reducing the fuel consumption and the related CO_2 emissions from gasoline engines in automobiles; a lean burn engine can decrease fuel consumption up to 30% compared with a stoichiometric engine (1). However, under lean conditions NO_x cannot be purified sufficiently by the conventional three-way catalysts because of the presence of excess oxygen in the exhaust gas.

Recently catalysts for the selective NO_x reduction by hydrocarbons under an oxidizing atmosphere have been studied extensively (2–5). However, these catalysts have many serious limitations including low NO_x conversion and low N_2 selectivity, narrow temperature window and insufficient durability. A promising alternative approach to deal with NO_x removal under lean conditions is the NO_x storage-reduction (NSR) concept, which was developed and put into the market by Toyota recently (6–9). The NSR catalyst is used in an engine that operates alternatively under lean and rich conditions: during lean operation the nitrogen oxides in the exhaust gas are stored on the catalyst, and during rich operation the stored NO_x is reduced to nitrogen. Successive sequences of long lean and short rich operation periods provide high efficiency for NO_x removal. A NSR catalyst consists of a high surface area support, such as γ-alumina, a noble metal, and a NO_x storage component, typically an alkaline or an alkaline earth compound.

Takahashi *et al.* (8) found that the amount of NO_x stored increases with increasing oxygen content in the gas phase. These authors provided IR evidence that NO_x is stored in the form of nitrates and suggested that NO_x is oxidized on precious metals and reacts with neighboring NO_x storage compounds to form nitrates. They also concluded that the reduction of NO_x to N_2 during rich conditions takes place at noble metal sites. The NO_x storage capacity is deteriorated by sulphur. The chemical composition of the NO_x storage compound was optimized to inhibit the growth in size of sulphate particles, so that the improved catalysts showed sufficient durability in the Japanese 10–15 mode test (using regular gasoline containing 30 ppm of sulphur compounds). The methods to improve the tolerance against sulphur poisoning of NSR catalysts were further and specifically addressed by Matsumoto *et al.* (10). Bogner *et al.* (11) investigated the performances of NSR catalysts using both synthetic and engine exhausts. They concluded that

[1] To whom correspondence should be addressed. Fax: +39-02-7063. 8173. E-mail: pio.forzatti@polimi.it.

0021-9517/01 $35.00

NO is oxidized to NO_2 on Pt under lean conditions and the latter is subsequently adsorbed in the form of a surface nitrate species; upon switching to a short, rich stoichiometric excursion the adsorbed NO_x decomposes, and NO is released and subsequently reduced by precious metal component. Fridell *et al.* (12) investigated the influence of key process parameters on the performances of barium oxide-based NSR catalysts. They reported maximum NO_x storage at about 380°C, a small increase in stored NO_x with increasing oxygen concentration, little difference with respect to the reducing agent (C_3H_6, C_3H_8, CO, or H_2), limited decrease in the presence of CO_2, significant NO desorption peaks immediately after the switch from lean to rich conditions, and IR evidence for nitrates when NO_x was stored and for isocyanates when the catalysts were regenerated under rich conditions in the presence of hydrocarbons. Mahzoul *et al.* (13) investigated the storage capacity of several NSR catalysts and suggested that two kinds of a site operate: a Pt site far from Ba crystallites behaving as oxidation center and a Pt site close to Ba crystallites responsible for nitrate formation.

The NSR concept has also been applied recently in the electricity generating industry at small–medium size plants (5–32 MW) under the trade name SCONOx. This process uses a platinum/alkaline or alkaline earth carbonate/alumina catalyst for the combined removal of NO_x, CO, and volatile organic compounds (VOC). The catalyst is reported to work by simultaneously oxidizing CO to CO_2, VOC to CO_2, NO to NO_2, and then absorbing NO_2 during the oxidation–absorption cycle. Regeneration of the catalyst is accomplished by passing a hydrogen (or hydrocarbon) reducing gas diluted with steam across the catalyst in the absence of oxygen. The hydrogen reacts with the adsorbed NO_x to form N_2 and H_2O. Hydrogen is generated at the site with a small reformer that uses natural gas and steam as input streams. Because the regeneration cycle must take place in an oxygen-free environment, the section of the catalyst undergoing regeneration must be isolated from the exhaust gas by using sets of louvres and valves. A SCOSOx catalytic coating can also be added to the oxidation catalyst to effectively remove SO_2 from the exhaust gas. If an SO_2 adsorbent is added, H_2S is formed during catalyst regeneration. Regeneration gases are then passed through an H_2S scrubber to remove the captured sulphur. The SCONOx process is typically applied to exhaust gas with low NO_x concentration as that generated by gas turbines equipped with advanced low dry NO_x burners allows achieving NO_x emissions as low as 1 ppm and eliminates the ammonia reagent found in the SCR technology (14, 15). Recently the U.S. Environmental Protection Agency declared SCONOx as the lowest achievable emission rate technology for NO_x abatement.

In this paper we intend to gain a better and quantitative understanding of the NO_x storage chemistry that is still lacking. We have therefore used a model Pt–BaO/γ-Al_2O_3 catalyst and a simplified synthetic exhaust gas containing oxygen and nitrogen oxides and a reducing gas consisting of hydrogen, both together with He as inert carrier gas. The influence of water and carbon dioxide, which are typically present in the exhaust, was also investigated. Flow reactor studies were performed in a wide temperature range with transients between lean and rich conditions to clarify the dynamic characteristics of the process. The sequence of phases in the transient experiments was properly designed in the attempt to separate the effects associated with adsorption and desorption merely caused by changes in gas compositions from those associated with surface chemical reactions. Along these lines quantitative information on the set of reactions involved in the storage and reduction stages was derived. Besides, TPD experiments of the catalyst, upon different NO_x storage times and after reduction, were performed to better clarify the nature and the amount of the adsorbed species present on the catalyst during storage and after reduction, and the reaction sequence in the NO_x storage-reduction cycle.

EXPERIMENTAL

Catalysts Preparation and Characterization

The γ-alumina support was obtained by calcination at 700°C of a commercial alumina material (Versal 250 from La Roche Chemicals). The Pt/γ-Al_2O_3 (1/100 w/w) and Ba/γ-Al_2O_3 (20/100 w/w) samples were prepared by incipient wetness impregnation of the calcined alumina support with aqueous solutions of dinitrodiammine platinum (Stream Chemicals, 5% Pt in ammonium hydroxide) or barium acetate (Stream Chemicals, 98.5%). The powders were dried overnight at 80°C in air and then calcined at 500°C for 5 h (heating and cooling rate = 0.0167°C/s). The Pt–Ba/γ-Al_2O_3 (1/20/100 w/w) catalyst was prepared by incipient wetness impregnation of the Pt/Al_2O_3 (1/100 w/w) powder with an aqueous solution of barium acetate (Stream Chemical, 98.5%). The powders were dried overnight at 80°C in air and calcined at 500°C for 5 h.

DTA-TG experiments were performed on a Seiko Model 6003 Instrument with a heating rate of 0.25°C/s. FTIR spectra of the sample (KBr pressed disk method) were recorded by a Perkin-Elmer 147 FTIR spectrometer.

XRD spectra were collected on a Brüker D8 advanced instrument equipped with graphite monochromator on the diffracted beam. The mean crystal sizes of γ-Al_2O_3 and $BaCO_3$ were calculated by the Scherrer equation. Quantitative analysis of crystalline $BaCO_3$ has been performed by XRD using integrated intensity of the (440) reflection and γ-Al_2O_3 as a reference. Calibration curve has been obtained using mechanical mixtures of crystalline $BaCO_3$ ((111) reflection of the orthorhombic modification) and Pt/γ-Al_2O_3 (1/100 w/w). Full width at half maximum and

integrated intensities have been extracted using a profile fitting commercial program.

Surface area and pore size distribution were determined by N_2 adsorption–desorption at 77 K with the BET method using a Micromeritics TriStar 3000 instrument. The Pt dispersion of the samples was estimated from hydrogen chemisorption at 0°C upon reduction in H_2 at 300°C using a TPD/R/O ThermoQuest instrument.

Catalytic Tests

The transient storage-reduction experiments were performed in a flow microreactor system by imposing step changes in the inlet reactants concentration and analyzing the transient response. In a typical experiment, the catalyst was loaded in the reactor and oxidized at 500°C for 1 h in He + 20% O_2. Then a stream of He + 3% O_2 (3.33 cm^3/s at standard temperature pressure, STP) was fed to the reactor and the catalyst temperature was set at the desired value (phase 1). After stabilization of the concentration signals a rectangular step feed of NO (1000 ppm) was admitted at constant temperature (phase 2). The NO_x storage proceeded up to catalyst saturation, and then the inlet NO concentration was stepwise decreased to zero (phase 3), and after stabilization of the NO_x signal at the reactor outlet the O_2 concentration was also decreased in a stepwise manner ideally to zero, in practice to about 100 ppm due to the presence of a trace amount of gaseous oxygen that was not possible to prevent (phase 4). The catalyst reduction was accomplished by imposing a stepwise perturbation in H_2 concentration (0 → 2000 ppm and 2000 → 0 ppm) at the inlet of the reactor (phases 5 and 6). Phase 1 was applied to obtain an oxidized catalyst surface, phase 2 represents the storage stage, phase 3 allowed for the desorption of labile stored NO_x, phases 4 and 6 realized a progressive change from oxidizing to reducing conditions and vice versa, thus preventing any undesired overlap between the storage and the reduction stages, and phase 5 represents the reduction phase. To study the effect of CO_2 and H_2O experiments were also performed using He + 1% H_2O, He + 0.3% CO_2, He + 3% CO_2, He + 0.3% CO_2 + 1% H_2O, and He + 3% CO_2 + 1% H_2O instead of pure He both in the exhaust and reducing gases. If not otherwise specified, the data reported in the paper were collected on fresh catalyst samples that were fully conditioned by performing few storage-reduction cycles until reproducible results could be obtained. The flow rates of the gases were measured and controlled by mass-flow controllers (Brooks 5850 TR), and the gases were mixed in a single stream before entering the reactor. The total flow rate of each phase was typically set at 3.33 cm^3/s STP. Two four-port valves were used to perform the abrupt switches between different phases. Care was taken to minimize all possible dead volumes in the lines before and after the reactor and in eliminating pressure and flow changes upon switching of the feed gases. The dead time measured for an inert tracer (Ar) was on the order of 2 s, and it was found negligible with respect to the characteristic times of the measured responses.

The reactor consisted of a quartz tube (7-mm internal diameter) directly connected to a mass spectrometer (Balzers QMS 200). 120 mg of catalyst with small particle diameter (100–120 μm) were used in each run in order to minimize diffusion limitations. The reactor was inserted into an electric furnace driven by a PID temperature controller/programmer (Eurotherm 2408). The temperature of the catalyst was measured and controlled by a K-type thermocouple (0.5-mm outer diameter) directly immersed in the catalyst bed.

The following mass-to-charge ratios were used to monitor the concentration of products and reactants: 2 (H_2), 18 (H_2O), 28 (N_2 or CO), 30 (NO), 32 (O_2), 44 (N_2O or CO_2), and 46 (NO_2). The mass spectrometer data were quantitatively analyzed using the fragmentation patterns and the response factors determined experimentally from calibration gases. Relevant interferences in the mass-to-charge signals were taken into account in determining the products composition. A gas chromatograph (HP 6890) equipped with a Poraplot Q and a 5 Å molecular sieve capillary column was also used for the analysis of CO_2, N_2O, and H_2O, and of O_2, N_2, and CO, respectively.

TPD experiments were performed both after different NO_x storage periods and after reduction with hydrogen. After NO_x storage or reduction of the stored NO_x at a given temperature the catalyst was first cooled to 200°C (cooling time 20 min) upon switching from the original atmosphere to He and then heated to 800°C in He (flow rate = 1 cm^3/s) at a rate of 0.25°C/s.

RESULTS AND DISCUSSION

Catalysts Characterization

The phases detected by XRD and their crystal size, along with surface area (S), pore volume (V), and average pore radius ($2V/S$) of the catalysts are listed in Table 1.

The Pt/γ-Al_2O_3 sample is characterized by a large surface area (210 m^2/g) and a large pore volume (1.15 cm^3/g). Impregnation of Pt/γ-Al_2O_3 with an aqueous solution of Barium acetate to prepare the Pt–Ba/γ-Al_2O_3 sample followed by drying and calcination at 500°C results in a significant reduction of the surface area (160 m^2/g vs 210 m^2/g) and of the pore volume (0.82 vs 1.15 cm^3/g), whereas the mean pore radius is only marginally affected if any.

In addition to γ-Al_2O_3 (JCPDS 10-425) traces of $BaCO_3$, both monoclinic (JCPDS 78-2057) and orthorhombic (whiterite, JCPDS 5-378) modifications have been detected in the fresh Pt–Ba/γ-Al_2O_3 (1/20/100 w/w) catalyst, whereas only the orthorhombic modification of $BaCO_3$ was observed in the Ba/γ-Al_2O_3 (20/100 w/w) catalyst. However, all the Ba-containing samples (both with and without Pt)

TABLE 1

Structural and Morphological Properties of the Catalysts

Catalyst	Phases (by XRD)	*d* crystallites (by XRD, Å)	Surface area *S* (BET, m^2/g)	Pore volume *V* (cm^3/g)	Pore radius $2V/S$ (Å)
Pt/γ-Al_2O_3 (1/100 w/w)	γ-Al_2O_3	≅70	210	1.15	110
Pt–Ba/γ-Al_2O_3 (1/20/100 w/w)	γ-Al_2O_3 $BaCO_3$ mon (tr) $BaCO_3$ orth (tr)	≅70 ≅70 ≅150	160	0.82	100
Ba/γ-Al_2O_3 (20/100 w/w)	γ-Al_2O_3 $BaCO_3$ orth (tr)	≅100 ≅140	140	0.80	114

kept in air for a long time showed only the presence of the stable orthorhombic modification of $BaCO_3$ (16). FTIR spectra confirmed the presence of carbonate species on the fresh catalyst (bands at 1420–1560, 1020–1060, and 620–660 cm^{-1}).

DTA-TG analyses in air showed the presence of an exothermic peak with an associated weight loss, that is ascribed to the thermal decomposition of Barium acetate, at 360–400°C in the case of Ba/γ-Al_2O_3 and at 270°C with only a small contribution at 360°C in the case of Pt–Ba/γ-Al_2O_3. The Pt-catalyzed decomposition of Barium acetate groups is responsible for the very fast and exothermic process observed at 270°C and for the appearance of the metastable monoclinic modification of $BaCO_3$.

The Pt dispersion, measured by H_2 chemisorption, is 90–95% in Pt/γ-Al_2O_3 (1/100 w/w), and 50–60% in Pt–Ba/γ-Al_2O_3 (1/20/100 w/w). The lower Pt dispersion in the latter sample is likely due to the fast and exothermic decomposition process of Barium acetate, which eventually causes sintering of the Pt crystallites, and/or masking of the Pt crystallites by the Ba component.

The quantitative analysis of XRD spectra indicates that the amount of crystalline $BaCO_3$ accounts for 5% of Ba in the fresh Pt–Ba/γ-Al_2O_3 (1/20/100 w/w) sample, and increases to 30% of Ba when the catalyst is kept in air at room temperature for seven months. Accordingly most of Ba is initially well dispersed on the surface of the catalyst and extensive surface restructuring occurs with time.

NO_x Storage-Reduction Experiments at 350°C

NO_x storage experiments. The results obtained during storage of NO_x in the presence of 3% oxygen (phases 1, 2, and 3) over the Pt–Ba/γ-Al_2O_3 (1/20/100 w/w) catalyst at 350°C are presented in Fig. 1. The data were collected after a few storage-reduction cycles were performed to fully condition the catalyst sample.

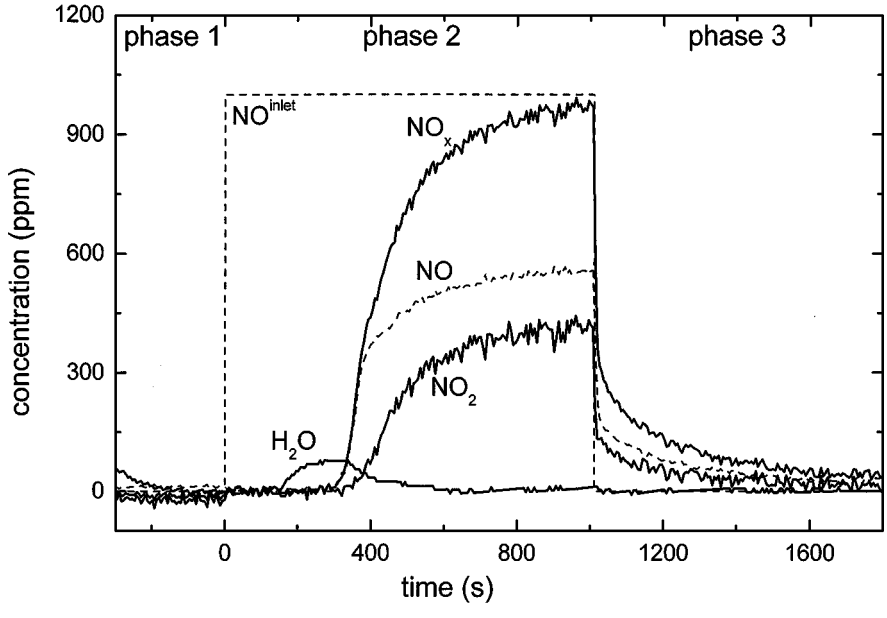

FIG. 1. Storage of NO_x over Pt–Ba/γ-Al_2O_3 (1/20/100 w/w) catalyst at 350°C: NO, NO_2, NO_x, and H_2O outlet concentration and NO inlet concentration with time.

Upon the NO step addition (at $t = 0$ s) the NO and NO_2 outlet concentrations showed a delay and then increased with time, approaching the asymptotic values corresponding to the NO inlet concentration (NO out + NO_2 out = NO_x out = NO in = 1000 ppm) at about 1000 s. The time delay is slightly greater for NO_2 (350 vs 290 s) and the variation in the outlet concentration upon breakthrough is slower. The area included between the inlet NO and outlet NO_x concentration traces is proportional to the amount of NO_x that has been stored onto the catalyst surface during phase 2. The storage of NO_x is accompanied by the release of a small amount of water after 150 s. Upon NO shutoff the concentrations of NO and of NO_2 decrease with time due to desorption of the NO_x previously stored. The net amount of NO_x that has been stored during phases 1, 2, and 3 is obtained by difference between the amount of NO_x that has been stored on the catalyst surface during phase 2 and the amount of NO_x that has been desorbed during phase 3. Upon switching from 3% O_2 in He (phase 3) to pure He (phase 4) a small quantity of NO is also desorbed (not shown in the figure). The results prove that NO_x is first adsorbed at BaO and then at $Ba(OH)_2$. The adsorption at $Ba(OH)_2$ is documented by the evolution of water; the time delay in the evolution of water indicates that this reaction is less favored than the previous one in line with the lower basic character of $Ba(OH)_2$.

In order to obtain additional information on the nature and reactivity of the Ba surface species involved in the NO_x storage process and on the transformation involved during catalyst conditioning the initial storage-reduction cycles performed over a fresh catalyst sample have been analyzed. The results collected in the three initial NO_x storage cycles performed at 350°C onto a fresh catalyst sample calcined in dry air at 500°C (*in-situ*) are presented in Fig. 2 in terms of NO_x, H_2O, and CO_2 outlet concentration as a function of time. In the first NO_x storage cycle (Section I of Fig. 2) upon the NO step addition at $t = 0$ s the NO_x outlet concentration presents a delay of about 50 s, and then slowly increases with time eventually reaching the inlet concentration value. An important evolution of CO_2 is also monitored with a time delay of about 50 s. The data prove that NO_x is first adsorbed at BaO and then at $BaCO_3$, in line with the greater basic character of the former site. Indeed IR analysis and XRD indicate that in the fresh calcined catalyst sample Ba is present as Ba carbonate. The catalyst pretreatment in dry air causes the decomposition of minor amounts of Ba carbonate and the evolution of small amounts of water, as shown by TPD analysis (data not reported). The decomposition of $BaCO_3$ in a dry environment leads to the formation of BaO. Accordingly $BaCO_3$ (that is predominant) and BaO, but not $Ba(OH)_2$, are present on the fresh catalyst upon calcination in dry air at 500°C. The second NO_x storage run (Section II of Fig. 2) has been performed after reduction with diluted H_2 at the same temperature and presents the following main features (i) the time delay in

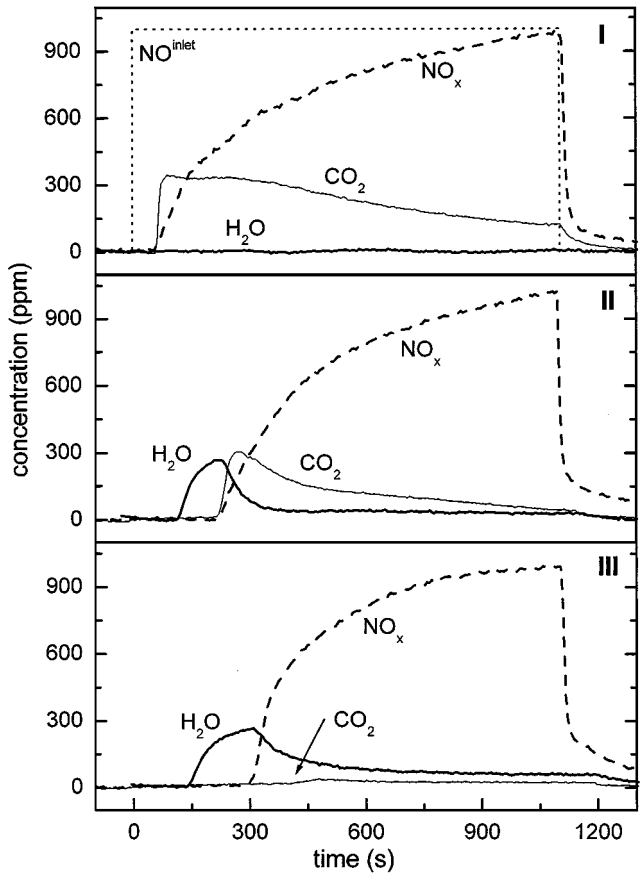

FIG. 2. Subsequent NO_x storage runs at 350°C on a fresh sample of Pt–Ba/γ-Al_2O_3 (1/20/100 w/w): NO_x, H_2O, CO_2 outlet concentration and NO inlet concentration.

the NO_x outlet concentration is greater (250 vs 50 s); i.e., the NO_x storage is enhanced; (ii) water evolution becomes evident and occurs with a time delay of 150 s; (iii) CO_2 evolution is significantly reduced and is now observed after 250 s. The data prove that the storage of NO_x occurs first at BaO, then at $Ba(OH)_2$, and finally at $BaCO_3$, in line with the basic character of the different Ba adsorption sites, and that the storage at $BaCO_3$ is of lower importance. Catalyst regeneration with H_2 restores the adsorption Ba sites; however, $Ba(OH)_2$ and BaO are formed instead of $BaCO_3$ since H_2O (and not CO_2) is produced during reduction (see below). Accordingly the amounts of BaO and $Ba(OH)_2$ species on the catalyst surface progressively increase at the expense of $BaCO_3$. The results obtained in the third NO_x storage cycle (Section III of Fig. 2), again performed after reduction with H_2 at 350°C, closely resembles those obtained over a fully conditioned sample (Fig. 1) and show that the NO_x adsorption is further enhanced with respect to the previous runs. Besides water evolution is increased whereas that of CO_2 is almost negligible because the transformation of $BaCO_3$ into BaO and $Ba(OH)_2$ has proceeded further, so that the catalyst is now close to being fully conditioned.

TPD of the catalyst after NO_x adsorption and after reduction. TPD experiments were performed to clarify the nature of the NO_x adsorbed species present on the catalyst surface upon storage, and the sequence of reactions involved in the NO_x storage process. Accordingly, TPD measurements were performed over the conditioned Pt–Ba/γ-Al_2O_3 (1/20/100 w/w) catalyst following NO_x adsorption at 350°C for different storage periods (60 and 120 s, before the NO_x breakthrough) and after reduction of the stored NO_x at 350°C.

The results of the TPD experiments are shown in Fig. 3. Upon heating the catalyst to 900°C complete desorption of the previously adsorbed NO_x was achieved. In all cases NO and O_2 represent the major products, along with negligible quantities of NO_2. NO is desorbed above 500°C after storage for 120 s, above 525°C after storage for 60 s, and above 500°C after reduction. The desorption of NO is accompanied by the evolution of O_2. NO_2 was observed only during TPD of the catalyst after extensive storage (not shown in the figure), namely after the end of phase 2, and was released at low temperature (T = 350–500°C); in this case the desorption of NO and O_2 is much greater and is detected starting from 350°C. The data indicate that the adsorption of NO_x results in the formation of less stable N-containing species as the storage process proceeds; indeed these species desorb at progressively lower temperature. Besides a limited amount of adsorbed NO_x, presumably the less reactive, does not take part in the storage-reduction cycle and remains adsorbed at the catalyst surface after all the reactive stored NO_x species have been reduced. The amounts of NO and of O_2 desorbed in the three cases are listed in Table 2. The net amounts of NO_x that has been stored for the different storage periods before the TPD run are also reported in the table; we note that no release of NO_x previously stored has been observed in all cases upon NO shutoff (phase 3).

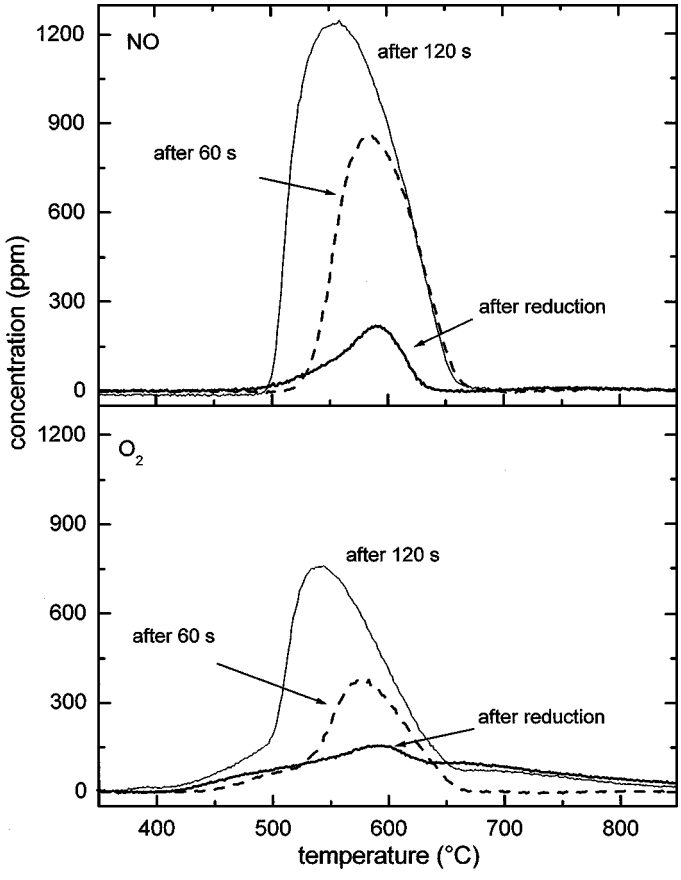

FIG. 3. TPD experiments of Pt–Ba/γ-Al_2O_3 (1/20/100 w/w) catalyst upon 120-s storage periods, 60-s storage periods, and after reduction: NO and O_2 traces.

It is worth noting that there is a reasonable correspondence in Table 2 between the amount of NO_x desorbed from the catalyst upon reduction (0.15×10^{-4} mol/g catalyst) and the amount of NO_x that is computed by difference between that desorbed during TPD upon different storage periods and that accumulated during the previous storage run (0.17×10^{-4} and 0.38×10^{-4} mol/g catalyst for storage periods of 60 and 120 s). It appears that the amount of this less reactive stored NO_x, that does not take part in the storage-reduction cycle, is limited and corresponds to less than 5–10% of the NO_x stored up to catalyst saturation.

During the TPD experiments NO, O_2, and NO_2 are likely produced through the following reactions:

$$Ba(NO_2)_2 \rightarrow BaO + 2\,NO + 1/2\,O_2 \quad [1]$$

$$Ba(NO_3)_2 \rightarrow BaO + 2\,NO + 3/2\,O_2 \quad [2]$$

$$Ba(NO_3)_2 \rightarrow BaO + 2\,NO_2 + O_2. \quad [3]$$

NO/O_2 molar ratios equal to 4.18 and 1.47 were measured during TPD of reference $Ba(NO_2)_2$ hydrate (Aldrich, technical grade 90%) and $Ba(NO_3)_2$ (Aldrich, pure grade 99.98%), in reasonable agreement with the values of 4 and 1.33 obtained from the stoichiometry of reactions [1] and [2] respectively. A negligible amount of NO_2 was measured in the latter case, indicating that either reaction [3] is not effective or NO_2 decomposes to NO and O_2.

In the TPD experiments shown in Fig. 3, O_2 evolution may also originate from the desorption of oxygen species associated with Pt sites (indicated below as O*) formed onto the catalyst surface in presence of excess oxygen:

$$2O^* \leftrightarrow O_2. \quad [4]$$

Assuming complete desorption of O* from fully oxygen covered Pt sites this reaction accounts approximately for 0.2×10^{-4} mol O_2/g catalyst.

Inspection of Table 2 indicates that the ratio between NO and O_2 decreases when the storage period increases from 60 to 120 s, which proves that the relative amount of nitrates increases progressively during storage. The amounts of nitrites and nitrates, estimated from the data in Table 2 on the basis of reactions [1], [2], and [4], depend

TABLE 2

TPD of Pt–Ba/γ-Al_2O_3 (1/20/100 w/w) in He upon Different Storage Periods at 350°C (60 and 120 s in He + 3% O_2 + 1000 ppm NO) and after Reduction at 350°C (in He + 2000 ppm H_2)

Type of experiment	NO desorbed (mol/g catalyst)	O_2 desorbed (mol/g catalyst)	NO_2 desorbed (mol/g catalyst)	NO_x adsorbed[a] (mol/g catalyst)
Upon storage (60 s)	0.91×10^{-4}	0.44×10^{-4}	0	0.74×10^{-4}
Upon storage (120 s)	1.88×10^{-4}	1.21×10^{-4}	0	1.5×10^{-4}
Upon reduction	0.15×10^{-4}	0.42×10^{-4}	0	—

[a] During the previous NO_x storage cycle.

markedly on the relevance of O* thermal desorption particularly in the case of short NO_x storage periods. It is expected that reaction [4] has occurred to a certain extent considering that the desorption of O_2 is detected already below 500°C (the temperature of onset of NO desorption); however, the relevance of this reaction cannot be assessed precisely from our data. Assuming that reaction [4] has occurred quantitatively the amount of nitrites calculated after a 60-s storage period is 0.84×10^{-4} mol/g catalyst and that of nitrates 0.07×10^{-4} mol/g catalyst. In this case the storage of NO_x should occur primarily through a stepwise oxidation of NO first to nitrites and then to nitrates. However, assuming that reaction [4] has not occurred at all from the same data we calculate 0.25×10^{-4} mol nitrites/g catalyst and 0.65×10^{-4} mol nitrates/g catalyst. In this case the storage of NO_x could be explained as well by oxidation of NO to NO_2, followed by dimerization of NO_2 to N_2O_4, disproportionation of N_2O_4 to form Ba-nitrites and Ba-nitrates, and finally oxidation of surface nitrites to nitrates as suggested in the technical literature (16). In any case the data in Table 2 indicate that the reactions of NO_2 at Pt sites close to BaO or $Ba(OH)_2$ to give $Ba(NO_3)_2$ are of lower importance in the NO_x storage process. The estimation of the relative amount of nitrates is less influenced by the poor confidence in the relevance of the thermal desorption of O* as the storage period increases because of the greater amount of stored NO_x. Accordingly, for the case of NO_x storage up to catalyst saturation a relative amount of nitrates ranging between 79 and 83% has been calculated. This confirms that nitrates are most abundant when the storage process has been completed. In conclusion the TPD study proved that nitrites are formed during storage and are oxidized to nitrates.

It was not possible to clarify whether nitrites are formed first and then are transformed into nitrates or nitrites and nitrates are formed first by disproportionation of N_2O_4 and nitrites are then oxidized to nitrates. However, it has been shown that the direct reaction of NO_2 to give $Ba(NO_3)_2$ is of lower importance. The present picture compares well with the results of a detailed FTIR study performed by some of us over the Pt–Ba/Al_2O_3 (1/20/100 w/w) catalyst upon contact with NO + O_2 at room temperature followed by evacuation at increasing temperature (17). This study provided evidence for the presence of a variety of surface species, including ionic bidentate nitrites coordinated at Ba^{2+}, monodentate nitrites, chelating and/or bridging bidentate nitrates, and ionic nitrates, and showed that the formation of nitrates is favored on contact time increase. Upon evacuation up to 400°C bidentate and monodentate nitrites progressively disappeared; besides bidentate nitrates were partially removed, and ionic Ba^{2+} nitrates were formed. Evacuation at 500°C caused the removal of bidentate nitrates and a fraction of ionic nitrates; the complete decomposition of these species required higher temperatures. TPD experiments performed upon contact at room temperature with NO + O_2 atmosphere showed a low temperature TPD peak (centerd at 250–300°C), that is ascribed to the removal of monodentate nitrites, bidentate nitrites, and bidentate nitrates and is not accompanied by oxygen evolution, and a high temperature peak (centerd at 550°C), that is accompanied by the evolution of oxygen and is ascribed to the elimination of the ionic Ba^{2+} nitrates with high thermal stability. In conclusion the FTIR study indicated that nitrites are transformed into nitrates and that ionic nitrates are the most stable species stored onto the catalyst.

NO_x storage chemistry. The results previously discussed indicate that the storage of NO_x occurs only at BaO and $Ba(OH)_2$ over the fully conditioned catalyst and results in the formation of nitrites and nitrates. Accordingly and in line with indications in the literature, the following reaction pathways can be considered to describe the NO_x adsorption processes on the conditioned Pt–Ba/Al_2O_3 catalyst:

$$O_2 \leftrightarrow 2O^* \quad [4']$$

$$BaO + O^* + 2NO \leftrightarrow Ba(NO_2)_2 \quad [5]$$

$$Ba(OH)_2 + O^* + 2NO \leftrightarrow Ba(NO_2)_2 + H_2O \quad [6]$$

$$Ba(NO_2)_2 + 2O^* \leftrightarrow Ba(NO_3)_2 \quad [7]$$

$$NO + 1/2O_2 \rightarrow NO_2 \quad [8]$$

$$BaO + 2NO_2 + O^* \leftrightarrow Ba(NO_3)_2 \quad [9]$$

$$Ba(OH)_2 + 2NO_2 + O^* \leftrightarrow Ba(NO_3)_2 + H_2O \quad [10]$$

$$2NO_2 \leftrightarrow N_2O_4 \quad [11]$$

$$2BaO + 2N_2O_4 \leftrightarrow Ba(NO_2)_2 + Ba(NO_3)_2 \quad [12]$$

$$2Ba(OH)_2 + 2N_2O_4 \leftrightarrow Ba(NO_2)_2 + Ba(NO_3)_2 + 2H_2O. \quad [13]$$

The storage of NO_x may proceed via three different reaction pathways. The first route (reactions [4′]–[7]) involves the adsorption of NO at Pt sites close to BaO or $Ba(OH)_2$ to form $Ba(NO_2)_2$ (reactions [5] and [6]) and then $Ba(NO_3)_2$ (reaction [7]). Reactions [5]–[7] imply the participation of active oxygen species, O^*, associated with oxidized Pt species, that are restored by gaseous oxygen (reaction [4′]). In the NO_x storage catalyst Pt is identified as the oxidation component and Ba as the NO_x storage component. Indeed experiments with 1000 ppm NO in He + 3% O_2 over Pt/γ-Al_2O_3 (1/100 w/w) demonstrated that this catalyst is able to oxidize NO to NO_2 although it presents a negligible capability to store NO_x. On the other hand it was found that Ba/γ-Al_2O_3 (20/100 w/w) is not able to catalyze the oxidation of NO to NO_2 and it does not adsorb NO to a significant extent even in the presence of oxygen. Besides previous reports in the literature have demonstrated that the migration process of NO_x from precious metals to the NO_x storage component is a very important step for NO_x storage, and that the migrated NO_x reacts with the NO_x storage component neighboring on precious metals (8). The second pathway (reactions [8]–[10]) considers $Ba(NO_3)_2$ formation via oxidation of NO to NO_2 (reaction [8]) followed by reaction of NO_2 at Pt sites close to BaO or $Ba(OH)_2$ (reactions [9] and [10]). Finally, the third route (reactions [8] and [11]–[13]) involves the oxidation of NO to NO_2 (reaction [8]), the dimerization of NO_2 to N_2O_4 (reaction [11]) and the disproportionation of N_2O_4 at BaO or $Ba(OH)_2$ to form $Ba(NO_2)_2$ and $Ba(NO_3)_2$ (reactions [12] and [13]) (15). Our data demonstrate that nitrites are formed during storage and then are oxidized to nitrates; accordingly the second route (reactions [8]–[10]) is of lower importance. Still the data do not allow us to distinguish whether nitrites are formed first and then are transformed into nitrates (reactions [5]–[7]) or nitrites and nitrates are formed at the same time by disproportionation of N_2O_4 and nitrites are subsequently oxidized to nitrates (reactions [8], [11]–[13], and [7]).

In the overall reaction scheme presented above, the reactions at $Ba(OH)_2$ (reactions [6], [10], and [13]) are less favored than the corresponding reactions at BaO (reactions [5], [9], and [12], respectively) and they occur at a lower extent, as documented by the time delay in the evolution of water and the release of a small amount of water during the NO_x storage (Fig. 1). The reactions given above also account for a number of features in Fig. 1 including (i) the storage of NO in the presence of O_2 through direct reactions [4′]–[7], and/or reactions [8], and [11]–[13], and/or, in minor extent, reactions [8]–[10]; (ii) the occurrence of NO_x storage first at BaO and then at $Ba(OH)_2$ since the former site is more basic in nature and in line with the results of the catalyst conditioning; (iii) the breakthrough of NO first and of NO_2 later on through reverse reactions [7] to [5], and reverse reaction [9], respectively. Storage experiments with 1000 ppm NO_2 in He under the same conditions and over Pt–Ba/γ-Al_2O_3 (1/20/100 w/w) confirmed that the desorption of NO is more favored than that of NO_2, since also in this case the breakthrough of NO_2 occurred later than that of NO; (iv) the sharp increase in gaseous NO concentration upon breakthrough and the more gentle increase of gaseous NO_2 concentration, since surface nitrite species are less stable than surface nitrate species; (v) the slow approach of the concentrations of NO and NO_2 to their asymptotic values due to the progressively lower relevance of direct reactions [5]–[13], as compared to reverse reactions [5]–[13]; (vi) the desorption of NO_x upon shutoff of NO through reverse reactions [7] and [5], reverse reactions [9] and [8], and reverse reactions [12], [11], and [8]; (vii) the desorption of NO upon switching from 3% O_2 in He to He primarily through reverse reactions [4′], [7], and [5].

Reduction of NO_x stored experiments. The results obtained during the reduction of stored NO_x (phases 5 and 6) over the Pt–Ba/γ-Al_2O_3 (1/20/100 w/w) catalyst at 350°C are presented in Fig. 4. Upon the step addition of 2000 ppm of H_2 at $t = 0$ s the stored NO_x is reduced to N_2 : H_2 is completely consumed and the N_2 outlet concentration increases immediately to the level of 360 ppm and then it keeps almost constant until depletion of reactive stored NO_x. Accordingly the reaction is very fast and is limited by the concentration of H_2. Besides the reduction of stored NO_x is highly selective toward N_2 since N_2O is not observed and only a very small amount of NO (not shown in the figure) is detected among the products immediately after the H_2 step addition (1.9×10^{-6} mol NO/g catalyst vs 2.36×10^{-4} mol N_2/g catalyst). The absence of N_2O is documented by the trace of mass-to-charge signal 44 and by direct GC analysis. The formation of NH_3 can also be ruled out by taking into account the interferences in the mass-to-charge signals 18 and 17. Accordingly selectivity toward nitrogen of about 99.5% is calculated from these data. The reduction of NO_x produces water, which, however, does not desorb immediately and indeed shows a delay of about 50 s, due to adsorption onto the catalyst and most likely onto Ba sites to form $Ba(OH)_2$. After the reduction of stored NO_x is completed and the N_2 outlet concentration diminishes to the background level approximately at 400 s, still the concentration of H_2O continues to decrease and that of H_2 continues to increase, approaching their asymptotic values only above 800 s. While the former effect could be due to desorption of water previously accumulated in the form of $Ba(OH)_2$, the latter effect indicates that H_2 is consumed to the expense of oxygen species different from stored NO_x that are

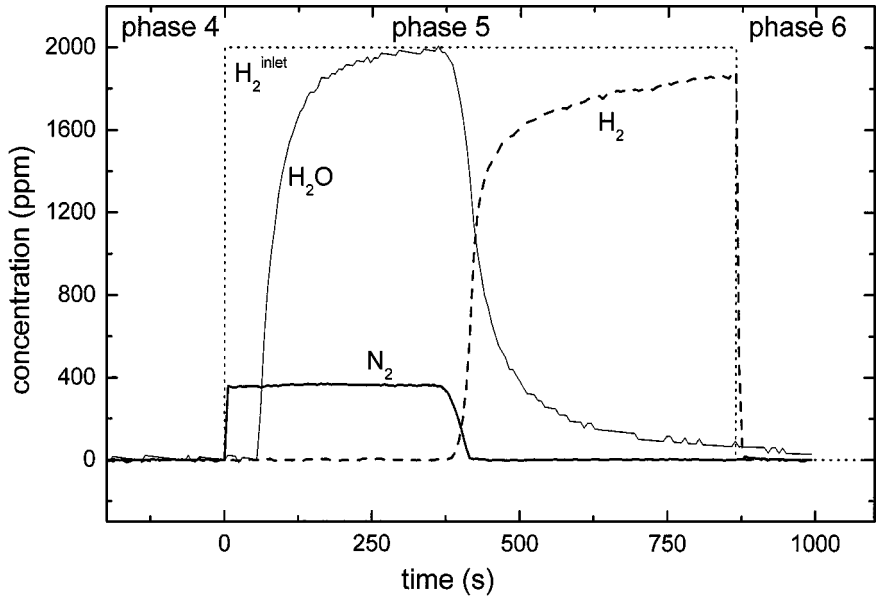

FIG. 4. Reduction of stored NO_x over Pt–Ba/γ-Al_2O_3 (1/20/100 w/w) catalyst at 350°C: H_2, N_2, and H_2O outlet concentration and H_2 inlet concentration.

progressively depleted and that are likely associated with poorly reactive oxygen species from the catalyst. One could speculate that such catalyst oxygen species are generated at the Ba sites through decomposition of nitrite/nitrate groups; in line with the lower reactivity of these species the reduction apparently operates after depletion of the stored NO_x groups. Overimposed to the consumption of these oxygen atoms and NO_x groups the reduction of trace amounts of gaseous oxygen in the feed (on the order of 100 ppm; see Experimental) is also observed, which eventually accounts for the asymptotic values of H_2 and H_2O concentration.

The following reactions are thus likely involved in the reduction of stored NO_x:

$$Ba(NO_2)_2 + 3H_2 \rightarrow BaO + N_2 + 3H_2O \quad [14]$$

$$Ba(NO_3)_2 + 5H_2 \rightarrow BaO + N_2 + 5H_2O \quad [15]$$

$$BaO + H_2O \leftrightarrow Ba(OH)_2 \quad [16]$$

$$O^* + H_2 \rightarrow H_2O \quad [17]$$

$$H_2 \leftrightarrow 2\,H^* \quad [18]$$

$$H_2 + 1/2O_2 \rightarrow H_2O \quad [19]$$

$$H_2 + O^{*\prime} \rightarrow H_2O. \quad [20]$$

$O^{*\prime}$ represents a poorly active oxygen species and H^* represents a hydrogen species associated to metal Pt. N_2 is produced by reduction of surface nitrites and nitrates (reactions [14] and [15]). Water, which is produced through these reactions, can react with BaO to form $Ba(OH)_2$ (reaction [16]). Notice that water is produced in excess of the amount that is required to fully hydrate the Ba sites made available through reactions [14] and [15], respectively, so that other Ba sites must be hydrated in order to account for the time delay of water. Water can also be adsorbed on the alumina support, but this can be considered of minor importance since Ba addition to the Pt/Al_2O_3 catalysts reduces significantly the exposed Al sites, as shown by FTIR analyses (17). Reduction of O^* to water, corresponding to the reduction of oxidized Pt species to Pt metal (reaction [17]), and the formation of H^* species from metal Pt (reaction 18), may also play a role in the process, in line with indications in the literature (18). Besides, the reduction of trace amounts of gaseous oxygen (reaction [19]) and poorly reactive oxygen species on the catalyst ($O^{*\prime}$) (reaction [20]) has also been considered (see above).

N and H material balances for the storage-reduction cycle (phase 1 to 6) in Figs. 1 and 4 close to within ±5–10%. It is worth noting that the N_2 concentration of 360 ppm in Fig. 4 corresponds to that expected from reaction [15] (360 ppm) and is significantly lower than that derived from reaction 14 (600 ppm); both expected values are computed taking into account the consumption of H_2 due to reduction of 100 ppm of gaseous oxygen. This eventually indicates that nitrates are most abundant when the storage process has been completed, and that the reduction of stored NO_x is very fast and almost complete with 2000 ppm H_2. Also the ratio of the moles of H_2 consumed to those of N_2 produced is consistent with the presence of major amounts of nitrates, based on the stoichiometry of reaction [15].

NO_x Storage-Reduction Experiments at Different Temperatures

The storage of NO_x in the presence of 3% oxygen over the conditioned Pt–Ba/γ-Al_2O_3 (1/20/100 w/w) sample has

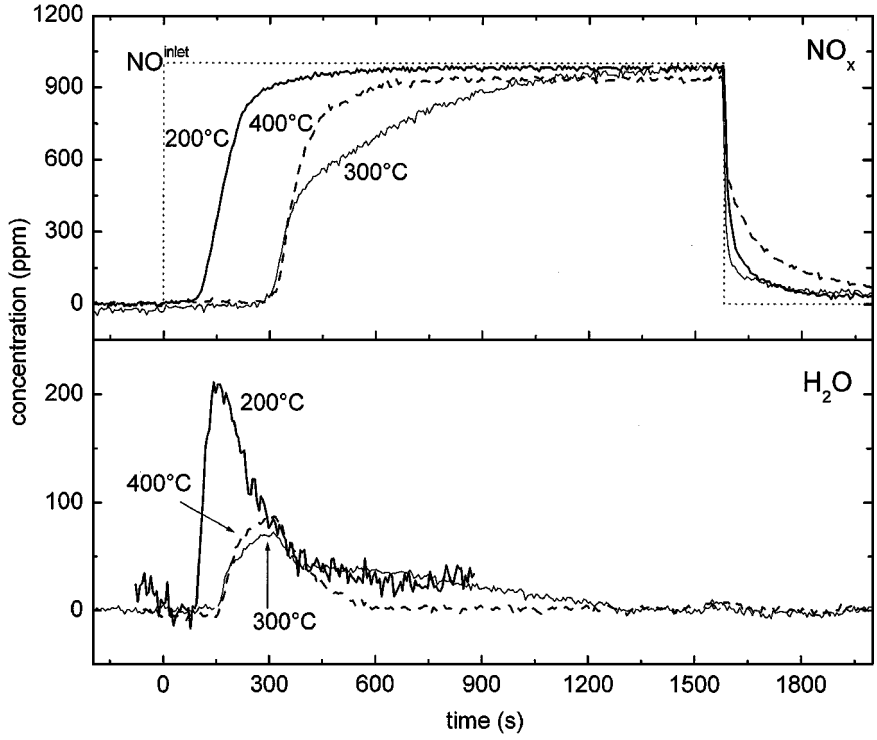

FIG. 5. Storage of NO_x over Pt–Ba/γ-Al_2O_3 (1/20/100 w/w) catalyst at different temperatures: NO_x and H_2O outlet concentration at 200, 300, and 400°C; NO inlet concentration.

been investigated in a wide temperature range, extending from 200 to 400°C. The results obtained during storage (phases 1, 2, and 3) at 200, 300, and 400°C are presented in Fig. 5. The time delay in the NO_x outlet concentration upon the NO step addition is largest at intermediate temperature and is maximum at 350°C (see Fig. 1); this originates from competition between the reactions responsible for the accumulation of nitrites and nitrates on the catalyst surface that are more favored at low temperature, and NO_x desorption upon decomposition of surface nitrites and nitrates that is more important at high temperature. After breakthrough the NO_x outlet concentration approaches the asymptotic value with higher rate the higher the temperature, again due to the greater relevance of the NO and NO_2 desorption processes. As the temperature increases the NO_2 outlet concentration gets closer to the thermodynamic limit for reaction [8]. During NO_x storage a small amount of water is released with a significant time delay, which indicates that also at these temperatures NO_x is first adsorbed at BaO and later on at $Ba(OH)_2$. Upon NO shutoff the release of a fraction of NO_x stored during phase 2 is observed; a small amount of NO is also monitored upon switching from 3% O_2 in He (phase 3) to He (phase 4) (not shown in the figure).

Calculations showed that considerable amounts of NO_x are stored onto the Pt–Ba/γ-Al_2O_3 (1/20/100 w/w) catalyst during the storage, up to 5.81×10^{-4} mol/g catalyst at 300°C. This amount is much greater than that reported by Fridell *et al.* under similar atmospheres (0.8×10^{-4} mol/g Al_2O_3 at 350–380°C), due to the larger surface area (160 vs 30 m^2/g) and the higher Pt dispersion (0.5–0.6 vs 0.18–0.27) of our catalyst, and in spite of the lower Ba content (Pt/Ba/Al 1/20/100 vs Rh + Pt/Ba/Al 1 + 2/20/77) (12). Indeed it is expected that the number of active sites for the NO_x oxidation reactions and for the activation of the reducing agent increases on increasing the Pt surface area (8) and that higher specific surface areas of the adsorbent component favor the storage of NO_x. The amount of NO_x stored onto the catalyst in the present study is comparable to that reported by Mahzoul *et al.* (13) for a commercial type catalyst containing Pt, Rh, Ba, and La supported on a washcoat base and operated under similar conditions (5.3×10^{-4} mol/g catalyst at 300°C in He + 3–7% O_2). The Ba percentages that participate in the storage process are estimated assuming the formation of $Ba(NO_2)_2$ and $Ba(NO_3)_2$ and are reported in Table 3. The percentage of Ba involved up to catalyst saturation (end of phase 2) shows a maximum of about 24% at 300°C. The percentage of Ba that is involved up to the NO_x breakthrough is also relevant for practical purposes; this is significantly lower at any temperature and increases with temperature to about 14% at 300°C, and then it levels off. The relative amounts of $Ba(OH)_2$ involved in the NO_x storage process is large (≅50–60%) at low temperature but diminishes significantly with temperature (down to 10–15%), as expected.

TABLE 3

% Ba Involved in the NO_x Storage Process up to Catalyst Saturation (phases 1 + 2 + 3 + 4) (% Ba Storage) and up to the NO_x Breakthrough (% Ba Breakthrough), and Relative Amounts of $Ba(OH)_2$ Taking Part in the Storage of NO_x ($Ba(OH)_2$/Ba Storage) over Pt–Ba/γ-Al_2O_3 (1/20/100 w/w) at Different Temperatures

Temperature	200°C	250°C	300°C	320°C	350°C	400°C
% Ba storage	7.3	15.5	23.8	22.5	16.7	13.3
% Ba breakthrough	4.1	7.4	13.7	13.4	14.7	13.0
$Ba(OH)_2$/Ba storage	62	53	10	10	11	14

The results obtained during the reduction of stored NO_x (phases 5 and 6) at 200, 300, and 400°C are presented in Fig. 6. The reaction is very fast and is limited by the concentration of H_2, already at 200°C. At any temperature the N_2 outlet concentration increases sharply to about 360 ppm, and then it keeps constant until depletion of the reactive stored NO_x. Small amounts of NO and of N_2O are observed at 200°C (2.7×10^{-6} mol NO and 2×10^{-6} mol N_2O/g catalyst vs 5.3×10^{-5} mol N_2/g of catalyst) and a more significant amount of NO is detected at high temperature (1.8×10^{-5} mol NO/g catalyst vs 1.41×10^{-4} mol N_2/g catalyst at 400°C). However, these amounts result in high selectivity toward N_2 that is close to 95% in both cases. The reactions responsible for the formation of NO and N_2O from surface nitrites and nitrates are (reactions [21]–[24]):

$$Ba(NO_2)_2 + H_2 \rightarrow BaO + 2NO + H_2O \quad [21]$$

$$Ba(NO_2)_2 + 2H_2 \rightarrow BaO + N_2O + 2H_2O \quad [22]$$

$$Ba(NO_3)_2 + 3H_2 \rightarrow BaO + 2NO + 3H_2O \quad [23]$$

$$Ba(NO_3)_2 + 4H_2 \rightarrow BaO + N_2O + 4H_2O. \quad [24]$$

Water is produced in the reduction and is adsorbed onto the Ba sites to form $Ba(OH)_2$. This eventually accounts for the observed delay in the outlet H_2O concentration; the time delay of water increases slightly with temperature. The traces of H_2O and H_2 continue to vary after the N_2 outlet concentration has diminished to zero, due to desorption of water previously accumulated in the form of $Ba(OH)_2$, and to the reduction of poorly reactive catalyst oxygen species (see above). The reduction of trace amounts of gaseous oxygen in the feed is also detected. Upon H_2 shutoff, a small but significant evolution of N_2 is observed at low temperature, namely at 200 and 250°C.

The formation of NO and N_2O at low temperature and NO at high temperature immediately after the H_2 step addition is likely associated with changes in the nature of the

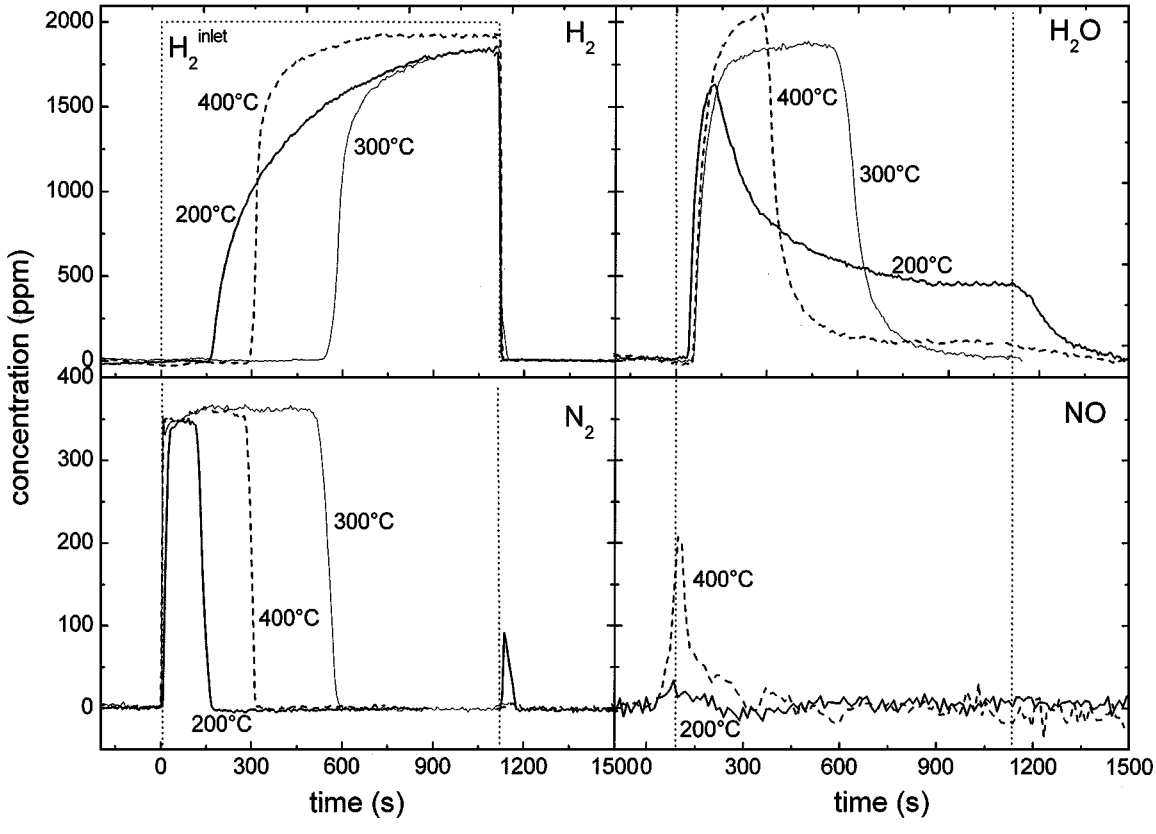

FIG. 6. Reduction of stored NO_x over Pt–Ba/γ-Al_2O_3 (1/20/100 w/w) catalyst at different temperatures: H_2, N_2, H_2O, and NO outlet concentrations at 200, 300, and 400°C; H_2 inlet concentration.

Pt species, i.e., from an oxygen-covered Pt to metal Pt and eventually to hydrogen-covered Pt. Accordingly when the reduction of oxygen adsorbed species (O*) is slow (low temperature) or the unselective reduction of NO_x is fast (high temperature) a lower selectivity to N_2 is measured, namely 95% at 200 and 400°C as compared to 99.5% at 350°C (see previous paragraph). The possibility that the evolution of NO could be due to thermal desorption caused by the increase of the catalyst temperature (3–5°C) upon the H_2 step addition has been ruled out on the basis of TPSR runs performed after NO_x storage in He + C_3H_6. Indeed TPSR experiments demonstrated that the temperature of onset of NO_x reduction is considerably lower than that employed in the storage-reduction cycles, in spite of the lower reducing power of propylene as compared to hydrogen.

Along similar lines the slow rate of reduction of precious metal sites combined with the more fast release of NO_x from the adsorbent has been suggested in the literature to account for the NO breakthrough peak observed upon switching from lean to rich conditions (11). However, for the same effect other authors have offered alternative explanations. Fridell *et al.* proposed that the reduction of the noble metal sites is fast and that the adsorption of NO_x on the reduced noble metal sites is strongly depressed, which eventually causes the NO breakthrough peak (12). It should be noted that the NO breakthrough peak upon switching from lean to rich conditions is much greater in intensity than the NO (+N_2O) peak observed when switching from He to He + H_2 feed, as observed in the present study, or from He to stoichiometric conditions, as reported in (9). In the latter case it has been argued that NO_x adsorbed on Pt/Ba catalyst in NO-O_2-H_2 reaction gas system was more reducible than that in NO-O_2-C_3H_6 reaction gas system due to the greater reduction power of H_2 than C_3H_6, which eventually accounts for the greater selectivity toward N_2. This applies more if O_2 is not present in the reaction gas as in the present study.

The evolution of small amounts of N_2 upon H_2 shutoff at 200°C is again likely associated with the changes in the nature of Pt species upon oxidation due to the presence of trace amounts of gaseous oxygen in the feed (from H-adsorbed species to metal Pt and finally to oxygen adsorbed species). Indeed the trace of oxygen increases to the background level with a small delay with respect to the H_2 shutoff that corresponds to the evolution of N_2. As a matter of fact it is speculated that metal Pt, formed immediately upon the H_2 shutoff, likely presents higher reactivity in the reduction of NO_x species that are still present on the catalyst so that few of them could be reduced to N_2.

NO_x Storage-Reduction Experiments in the Presence of CO_2 and H_2O

Effect of CO_2. Figure 7 illustrates the influence of 0.3% CO_2 on the NO_x storage at 200, 300, and 400°C during the lean phase for the Pt–Ba/γ-Al_2O_3 (1/20/100 w/w) catalyst. At any temperature the time delay in NO_x outlet concentration upon the NO step addition is remarkably reduced in the presence of 0.3% CO_2 (compare Fig. 7 with Fig. 5). Notably, no delay is observed in this case in the evolution of CO_2, suggesting that the catalyst surface is fully carbonated. Besides the desorption of part of the NO_x previously stored upon the NO shutoff is accompanied by a net

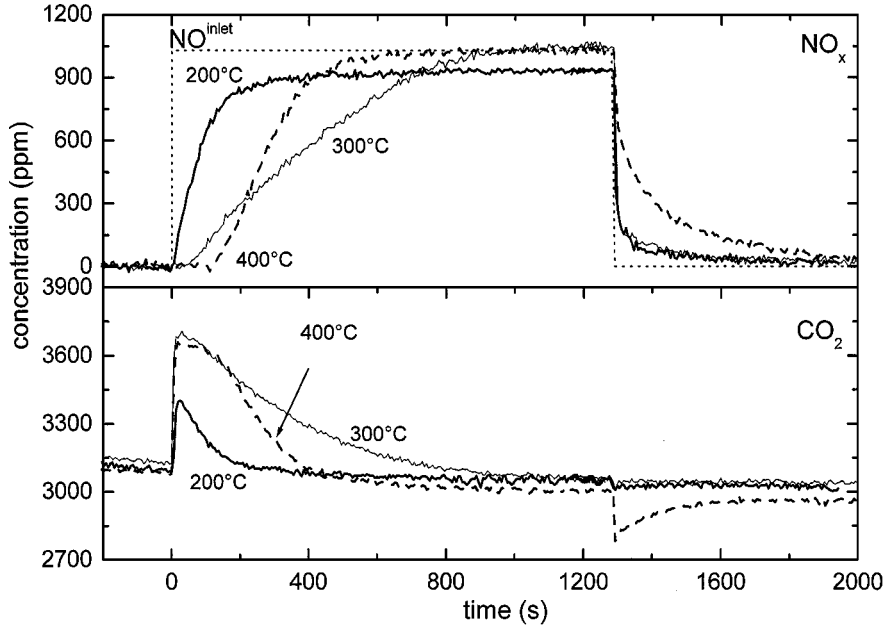

FIG. 7. Storage of NO_x over Pt–Ba/γ-Al_2O_3 (1/20/100 w/w) catalyst in the presence of 0.3% CO_2: NO_x and CO_2 outlet concentration at 200, 300, and 400°C; NO inlet concentration.

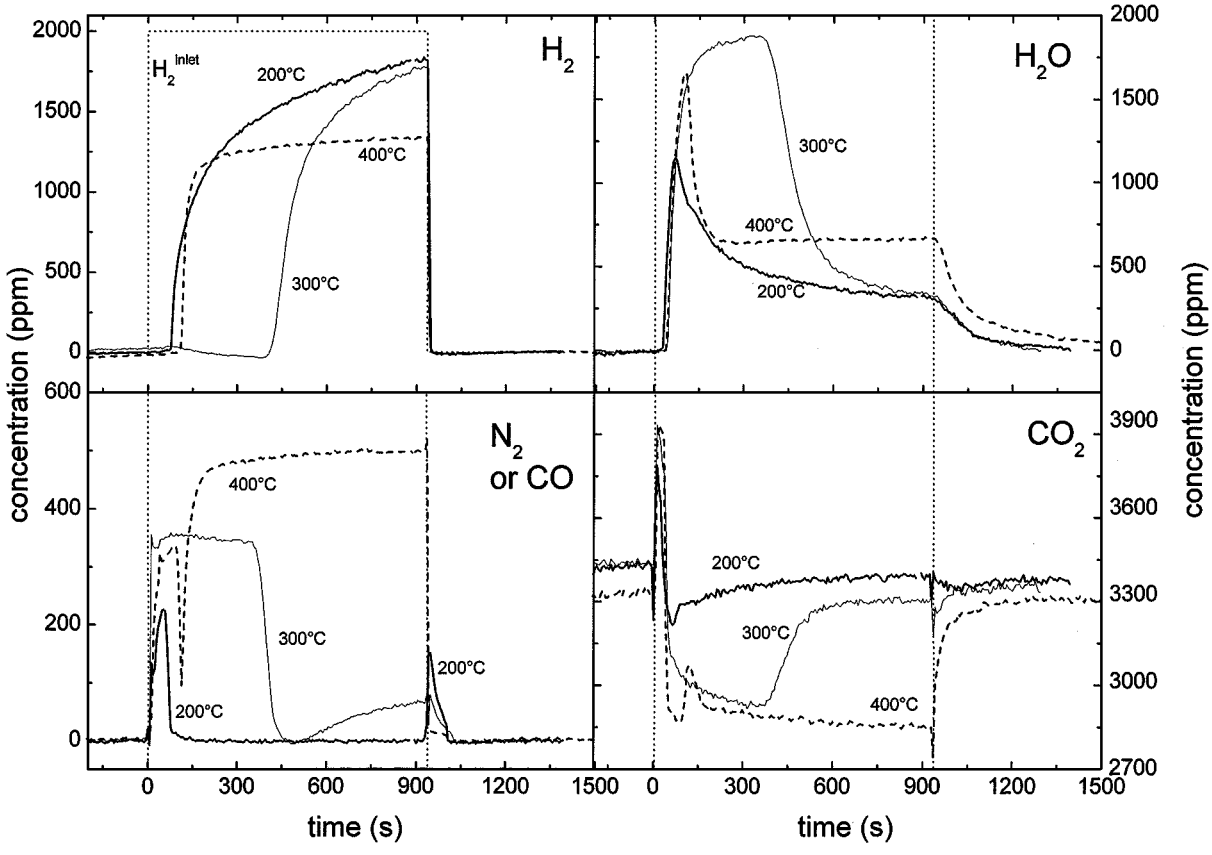

FIG. 8. Reduction of stored NO_x over Pt–Ba/γ-Al_2O_3 (1/20/100 w/w) catalyst in the presence of 0.3% CO_2: H_2, charge to mass ratio 28 (N_2 or CO), CO_2, and H_2O outlet concentration at 200, 300, and 400°C; H_2 inlet concentration.

consumption of CO_2. The net amount of NO_x that has been stored during phases 2 and 3 is significantly lower than in the absence of CO_2 and is twice the net amount of CO_2 that was released from the catalyst. The net quantity of NO_x stored is maximum at 300°C and amounts to 4.46×10^{-4} mol/g catalyst, which compares to 5.81×10^{-4} mol/g catalyst measured at the same temperature and in the absence of CO_2. This is consistent with previous studies (12), where it was reported that the amount of NO_x stored was decreased to a limited extent in the presence of 4.2–12% CO_2 at 400°C.

Considering that Ba sites are present in the form of $BaCO_3$ under the conditions of Fig. 7 it is believed that the storage of NO_x involves the following reactions:

$$BaCO_3 + 2NO + O^* \rightarrow Ba(NO_2)_2 + CO_2 \quad [25]$$

$$Ba(NO_2)_2 + 2O^* \rightarrow Ba(NO_3)_2 \quad [26]$$

$$2BaCO_3 + 2N_2O_4 \rightarrow Ba(NO_2)_2 + Ba(NO_3)_2 + CO_2. \quad [27]$$

Reactions [25] and [27] account quantitatively for the combined consumption of NO and release of CO_2 during phases 2 and 3. The shorter time delay in the NO_x breakthrough can be ascribed to the inhibiting effect of CO_2 on the overall storage process that is likely due to the participation of $BaCO_3$ in reactions [25] and [27].

The effect of CO_2 during the reduction of stored NO_x (phases 5 and 6) at different temperatures is presented in Fig. 8. The reaction is fast and H_2 is completely consumed immediately upon its addition. At any temperature the N_2 outlet concentration increases sharply to the maximum value of about 200 ppm at 200°C and of about 360 ppm at higher temperature, and then it keeps constant until depletion of the reactive stored NO_x. The reaction is limited by the H_2 concentration above 250°C (data not reported in the figure), but not at 200°C, where H_2 spillover must be invoked together with the inhibiting effect of CO_2 on the reduction of the stored NO_x to account for the complete consumption of H_2 and for the relatively low concentration of N_2 at the same time. The trace of the mass-to-charge signal 44, which is ascribed to CO_2, is complex: significant amounts of CO_2 are desorbed immediately after the addition of H_2; then CO_2 is consumed until depletion of stored NO_x. The desorption of CO_2 is likely due to the occurrence of the following reaction:

$$BaCO_3 + H_2O \rightarrow Ba(OH)_2 + CO_2. \quad [28]$$

Indeed water is produced through the reduction of stored

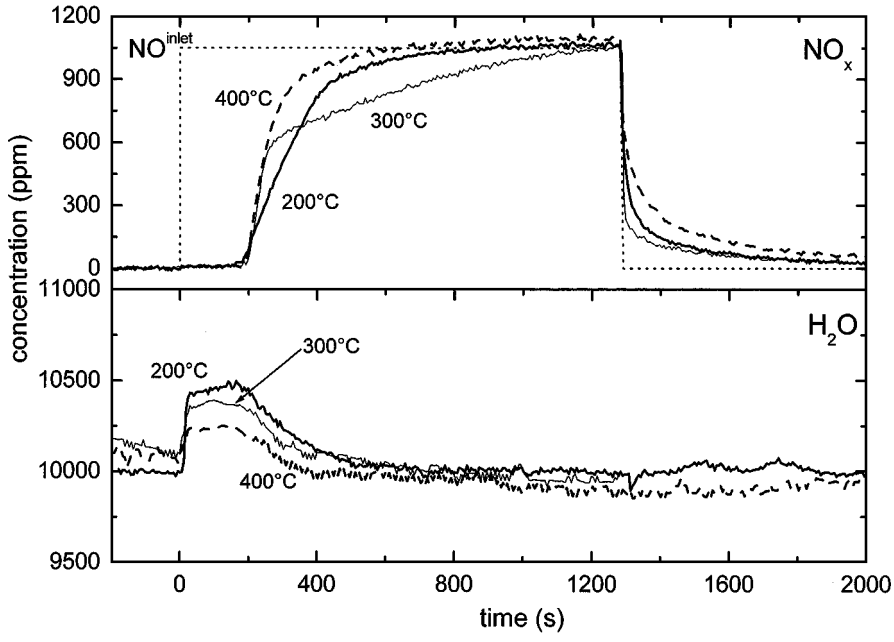

FIG. 9. Storage of NO_x over Pt–Ba/γ-Al_2O_3 (1/20/100 w/w) catalyst in the presence of 1% H_2O: NO_x and H_2O outlet concentration at 200, 300, and 400°C; NO inlet concentration.

NO_x and is detected at the reactor exit with a time delay of about 50 s, that compares well with the characteristic time of the desorption of CO_2. Likewise the consumption of CO_2 is ascribed to the reverse of reaction [28] which implies readsorption of CO_2 on $BaO/Ba(OH)_2$ once NO_x has been reduced.

After all stored reactive NO_x groups have been reduced and at sufficiently high temperature, i.e., at $T \geq 300$°C, the mass-to-charge signal 28 increases again and reaches an asymptotic value that is higher at high temperature. GC analyses confirmed that in this case the charge-to-mass signal 28 is associated with CO. The increase in the CO outlet concentration is accompanied by the parallel consumption of H_2 (the H_2 outlet concentration is lower at high T), and of CO_2 (the CO_2 trace does not recover the level corresponding to CO_2 feed concentration), and by the parallel production of H_2O (the H_2O trace keeps high until H_2 shutoff). It is therefore concluded that, after all stored reactive NO_x groups have been reduced and provided that the temperature is sufficiently high, the catalyst promotes the reverse water gas shift (WGS) reaction:

$$CO_2 + H_2 \Leftrightarrow CO + H_2O. \qquad [29]$$

The WGS reaction is limited by thermodynamics under the experimental conditions employed in this study, since the value of the reaction constant K_{sp} (based on the asymptotic concentration of reactants and products) is close to the value of the equilibrium constant K_{eq}.

Upon H_2 shutoff at low temperature (200°C) N_2 evolution is observed for reasons already discussed, and at any temperature the traces of carbon dioxide and water approach progressively their background levels, due to readsorption of CO_2 and desorption of H_2O (reverse reaction [28]). Storage-reduction experiments were also performed with synthetic exhaust and reducing gases containing 3% CO_2 at 300 and 350°C, and the same effects described above have been observed.

Effect of H_2O. The influence of water on the NO_x storage at 200, 300, and 400°C during the lean phase for the Pt–Ba/γ-Al_2O_3 (1/20/100 w/w) catalyst is presented in Fig. 9. The storage of NO_x is accompanied by a simultaneous release of water, because the adsorption of NO_x occurs primarily through reactions [6], [10], and [13] since in the presence of water in the gas phase the Ba component has been transformed into $Ba(OH)_2$. Notably, no dead time is observed in the evolution of water, thus suggesting that $Ba(OH)_2$ is predominant in these conditions. The relatively small variations in the concentration of water and experimental limitations on the recording of the trace of H_2O did not allow us to verify at a quantitative level the correspondence between the amount of water released and that of NO_x stored, as dictated by the stoichiometry of the reactions. Besides, a striking effect of water is that it causes an increase of the time delay of NO_x outlet concentration at low temperature and a decrease at high temperature (compare Figs. 5 and 9). It seems that water has a promoting action at low temperature and a negative effect at high temperature on the reactions involved in the NO_x storage process. The net amount of NO_x stored up to catalyst saturation in the presence of water is lower by 20–40%

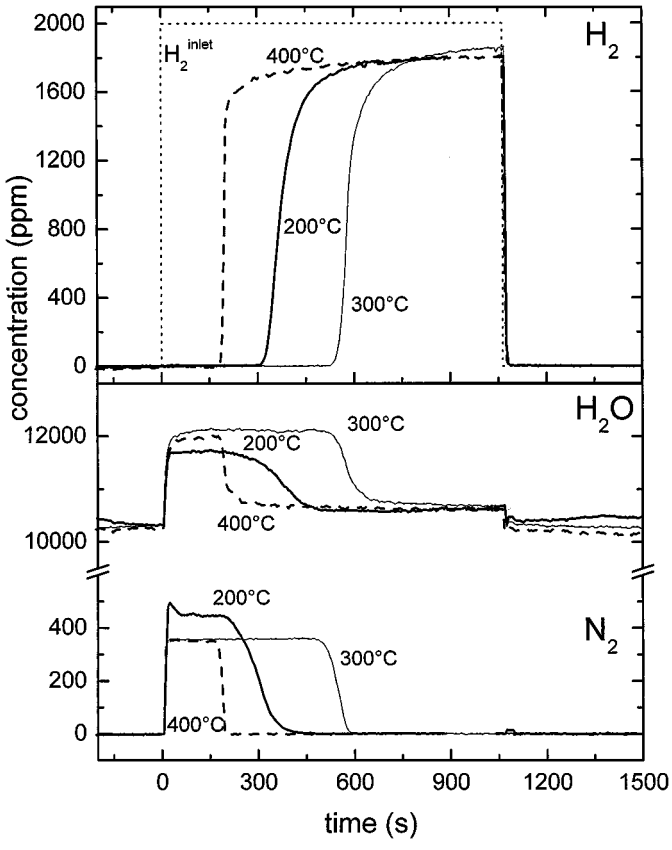

FIG. 10. Reduction of stored NO_x over Pt–Ba/γ-Al_2O_3 (1/20/100 w/w) catalyst in the presence of 1% H_2O: H2, N_2, and H_2O outlet concentration at 200, 300, and 400°C; H_2 inlet concentration.

at any temperature, except at 200°C where the amount is greater.

The effect of H_2O during the reduction of stored NO_x at 200, 300, and 400°C is presented in Fig. 10. The reaction is fast and H_2 is fully consumed immediately upon its addition. Besides, the reaction is highly selective since NO and N_2O were not detected, not even in trace amounts, during reduction. Note that at 200°C immediately upon the H_2 step addition the outlet N_2 concentration of about 500 ppm has been detected, which suggests that nitrites are present in significant amounts upon NO_x storage up to catalyst saturation. Indeed 500 ppm N_2 is a concentration significantly higher than that expected for the reduction of nitrates (400 ppm, from reaction [15]), even neglecting the consumption of H_2 due to the reduction of trace amounts of gaseous oxygen, and is lower than that expected for the reduction of nitrites (600 ppm, from reaction [14]), considering in this case the consumption of hydrogen caused by the reduction of trace amounts of gaseous oxygen. This implies that water inhibits the reactions responsible for the formation of nitrates. Still the promoting effect of water at low temperature on NO_x stored up to the NO_x breakthrough and up to catalyst saturation might be associated with the participation of surface hydroxyls in the storage process. This aspect deserves further study and it will be investigated in the future.

Combined effect of CO_2 and H_2O. The combined effect of 0.3% CO_2 and 1% H_2O on the NO_x storage capacity of the catalyst up to the NO_x breakthrough is summarized in Table 4, where also the data obtained in the absence of CO_2 and H_2O, in the presence of 0.3% CO_2, and in the presence of 1% H_2O are listed for comparison. It appears that the amount of NO_x stored is much lower in the presence of 0.3% CO_2 if compared to the case of He + 3% O_2 at any temperature and is almost negligible at 200 and 250°C. Likewise the amount of NO_x stored is more significant in the presence of 1% H_2O, and at 200 and 250°C it is even greater than that observed in the case of He + 3% O_2. The effects of 0.3% CO_2 and 1% H_2O tend to compensate each other when both species are present, and this eventually results in a lower but still significant storage capacity of the catalyst at any temperature: the storage capacity up to the NO_x breakthrough is reduced approximately by a factor of 2 and varies from 0.54×10^{-4} to 1.89×10^{-4} mol/g catalyst whereas in the case of He + 3% O_2 it varies from 1.01×10^{-4} to 3.60×10^{-4} mol/g catalyst. The above numbers correspond to Ba percentages varying from 2.2 to 7.8% in the presence of 0.3% CO_2 + 1% H_2O, which compare with Ba percentages between 4.1 and 14.7% in the case of He + 3% O_2.

The net amount of NO_x stored up to saturation of the catalyst is shown in Table 5 for the different feed compositions. This quantity is lower in the presence of 0.3% CO_2 and is more significant in the presence of 1% H_2O, particularly at low temperature, when compared to the case of He + 3% O_2. Again in the presence of 0.3% CO_2 + 1%

TABLE 4

Effect of 0.3% CO_2, 1% H_2O, and 0.3% CO_2 + 1% H_2O on the Amount of NO_x Stored up to the NO_x Breakthrough (mol/g Catalyst) over Pt–Ba/γ-Al_2O_3 (1/20/100 w/w) Catalyst

Temperature	Base (He + 3% O_2)	+0.3% CO_2	+1% H_2O	+0.3% CO_2 + 1% H_2O
200°C	1.01×10^{-4}	0.0	2.11×10^{-4}	0.54×10^{-4}
250°C	1.81×10^{-4}	0.0	2.29×10^{-4}	0.97×10^{-4}
300°C	3.35×10^{-4}	0.31×10^{-4}	2.38×10^{-4}	1.19×10^{-4}
350°C	3.60×10^{-4}	0.95×10^{-4}	2.77×10^{-4}	1.07×10^{-4}
400°C	3.17×10^{-4}	1.41×10^{-4}	2.44×10^{-4}	1.89×10^{-4}

TABLE 5

Effect of 0.3% CO_2, 1% H_2O, and 0.3% CO_2 + 1% H_2O on the NO_x Stored up to Catalyst Saturation (mol/g Catalyst) over Pt–Ba/γ-Al_2O_3 (1/20/100 w/w) Catalyst

Temperature	Base (He + O_2)	+0.3% CO_2	+1% H_2O	+0.3% CO_2 + 1% H_2O
200°C	1.77×10^{-4}	0.82×10^{-4}	3.76×10^{-4}	0.99×10^{-4}
250°C	3.79×10^{-4}	3.19×10^{-4}	3.28×10^{-4}	1.66×10^{-4}
300°C	5.81×10^{-4}	4.46×10^{-4}	4.60×10^{-4}	3.55×10^{-4}
350°C	4.07×10^{-4}	3.40×10^{-4}	4.16×10^{-4}	4.31×10^{-4}
400°C	3.24×10^{-4}	2.04×10^{-4}	2.48×10^{-4}	2.71×10^{-4}

H_2O the above effects compensate each other so that the net amount of NO_x stored up to catalyst saturation is lower roughly by 20–40% and varies from 0.99×10^{-4} to 4.31×10^{-4} mol/g catalyst whereas in the case of He + 3% O_2 it varies from 1.77×10^{-4} to 5.81×10^{-4} mol/g catalyst.

Storage-reduction experiments were also performed with synthetic exhaust and reducing gases containing 3% CO_2 and 3% CO_2 + 1% H_2O at 300 and 350°C. It has been observed that the amount of NO_x stored up to the breakthrough and up to catalyst saturation is not markedly affected on increasing the CO_2 content from 0.3 to 3% both in the presence and in the absence of water. Besides the reverse WGS reaction is limited by thermodynamics; accordingly the formation of CO is markedly depressed in the presence of water.

CONCLUSIONS

The results presented in this paper, and particularly those collected during catalyst TPD upon different storage periods, demonstrate that nitrites are formed during storage of NO_x over Pt–Ba/Al_3O_3 and then are oxidized to nitrates. Still the data do not allow us to distinguish whether nitrites are formed first and then are transformed into nitrates or nitrites and nitrates are formed at the same time by disproportionation of N_2O_4 and nitrites are subsequently oxidized to nitrates. In any case nitrates are most abundant and account for about 80% of the stored NO_x when the storage process is completed. The N_2 outlet concentration measured during subsequent reduction is also consistent with the predominance of nitrates at the end of the NO_x storage. In the presence of 1% H_2O in the exhaust and at low temperature (i.e., 250°C) there is evidence that nitrites are also present in significant amounts. 1% H_2O has a promoting effect at low temperatures and an inhibiting effect at high temperature on the reactions involved in the NO_x storage process. The presence of nitrites at low temperature could be ascribed to the promoting role of surface hydroxyls in the process, which would favor the adsorption of NO_x in the form of nitrites but not the subsequent oxidation of nitrites to nitrates. 0.3–3% CO_2 has always a marked inhibiting effect on the storage of NO_x. The storage of NO_x is inhibited in the presence of 1% H_2O and 0.3–3% CO_2 at any temperature. Our data are consistent with results previously published in the literature suggesting that NO_x is stored in an oxidized form, but they also indicate, at variance with the most common picture presented in the literature, that the direct absorption of NO_2 upon oxidation of NO to NO_2 is of lesser importance (8, 9, 11–13).

The storage of NO_x occurs first at BaO and then at $Ba(OH)_2$ in He + 3% O_2 atmosphere, in line with the greater basic nature of the former compound. Under these conditions $BaCO_3$, which was originally present in the fresh catalyst, is transformed into $Ba(NO_2)_2$ and $Ba(NO_3)_2$ during NO_x storage and then into BaO and $Ba(OH)_2$ upon subsequent reduction. As expected the relative amount of $Ba(OH)_2$ diminishes significantly with temperature. However, in the presence of 1% H_2O and/or 0.3–3% CO_2 all the Ba sites are transformed into $Ba(OH)_2$ and/or $BaCO_3$, and the storage of NO_x is accompanied by the release of H_2O and CO_2 in stoichiometric amounts. From these results as well as from information collected during catalyst conditioning it is concluded that the following order of stability applies for the different Ba species present in the NSR cycle, in line with their increasing acid character ($BaSO_4$ is formed in the presence of SO_2 in the exhaust):

$$BaO < Ba(OH)_2 < BaCO_3 < BaNO_2 < BaNO_3 < BaSO_4.$$

Considerable amounts of NO_x is stored onto the Pt–Ba/γ-Al_2O_3 catalyst when operating under He + 3% O_2 atmosphere, up to 5.81×10^{-4} mol/g catalyst at 300°C corresponding to 24% Ba involved in the storage. In the presence of 1% H_2O the amount of stored NO_x is slightly higher at low temperature and lower at high temperature. CO_2 has a marked inhibiting effect at low temperature, and only a limited effect at high temperature. It is worth noting that the inhibiting effect of CO_2 operates already at low concentrations, namely at 0.3% CO_2, and is not significantly modified on further increases in CO_2 content. In the presence of 0.3% CO_2 + 1% H_2O the amount of NO_x stored up to catalyst saturation was lower by roughly 20–40%.

The amount of NO_x that is stored onto the catalyst up to the NO_x breakthrough is also of practical importance.

This quantity is markedly affected by the composition of the exhaust gas and corresponds best to 13–15% Ba at 300–400°C in He + 3% O_2 atmosphere. In the presence of CO_2 it is much lower, and almost negligible at low temperatures, whereas it is more relevant in the presence of water. In the presence of both 1% H_2O and 0.3–3% CO_2 the percentage of Ba involved up to the NO_x breakthrough varies from 2.2 to 7.8%, which corresponds to a reduction by a factor of 2 when compared to the case of He + 3% O_2 atmosphere.

It is worth noticing that the amounts of NO_x that are stored up to the NO_x breakthrough and up to catalyst saturation specified above do not include a limited but significant amount of stored NO_x that does not take part in the storage-reduction cycle and remains adsorbed onto the catalyst after all the reactive stored NO_x species have been reduced.

The reduction of stored NO_x in He + 2000 ppm H_2 is very fast and is limited by the concentration of H_2 at any investigated temperature, and already at 200°C. The reaction is highly selective toward N_2; very small amounts of NO and of N_2O and small amounts of NO are detected, respectively, at low and high temperature. Selectivity always in excess of 95%, and close to 100% in most cases, was measured. The formation of NO and N_2O at low temperatures and NO at high temperatures immediately after the H_2 step addition is likely associated with the reduction of oxygen-covered Pt to the metal. Indeed the oxidized precious metal is not efficient in the reduction of NO_x to N_2 so that when the reduction is slow (low temperature) or the undesired reactions leading to NO and N_2O are fast (high temperature) a lower selectivity to N_2 is measured. Along similar lines the evolution of small amounts of N_2 upon H_2 shutoff at 200°C could be associated with the changes in the nature of Pt species, possibly oxidation from H-covered Pt to metal Pt, and eventually to oxygen covered Pt due to the presence of trace amounts of gaseous oxygen in the feed.

The reduction of stored NO_x is inhibited in the presence of 0.3–3% CO_2 and 0.3–3% CO_2 + 1% H_2O. Besides in the presence of CO_2, at sufficiently high temperatures ($T \geq 300$°C) and once all the stored reactive NO_x has been reduced, CO is formed through the reverse WGS reaction that is catalyzed by the noble metal component. However, the reverse WGS reaction is of limited importance in the presence of large concentrations of water in the exhaust because it is constrained by thermodynamics.

ACKNOWLEDGMENT

This work was supported by MURST (Roma)—Cofin 2000: Project "Catalysis for the Reduction of the Environmental Impact of Mobile Sources."

REFERENCES

1. Heck, R. M., and Farrauto, R. J., "Catalytic Air Pollution Control." Van Nostrand–Reinhold, New York, 1995.
2. Sato, S., Yu.-u, Y., Yahiro, H., Mizuno, N., and Iwamoto, M., *Appl. Catal.* **70**, L1 (1991).
3. Iwamoto, M., and Hamada, H., *Catal. Today* **10**, 51 (1991).
4. Burch, R., Millingbton, P. I., and Walker, A. P., *Appl. Catal. B: Environ.* **4**, 65 (1994).
5. Shelef, M., *Chem. Rev.* **95**, 209 (1995).
6. Miyoshi, N., Matsumoto, S., Katoh, K., Tanaka, T., Harada, J., Takahashi, N., Yokota, K., Sugiura, M., and Kasahara K., SAE Technical Paper 950809, 1995.
7. Matsumoto, S., *Catal. Today* **29**, 43 (1996).
8. Takahashi, N., Shinjoh, H., Iijima, T., Szuki, T., Yamazaki, K., Yokota, K., Suzuki, H., Miyoshi, N., Matsumoto, S., Tanizawa, T., Tanaka, T., Tateishi, S., and Kasahara, K., *Catal. Today* **27**, 63 (1996).
9. Shinjoh, H., Takahashi, N., Yokota, K., and Sugiura, M., *Appl. Catal. B: Environ.* **15**, 189 (1998).
10. Matsumoto, S., Ikeda, Y., Suzuki, H., Ogai, M., and Miyoshi, N., *Appl. Catal. B: Environ.* **25**, 115 (2000).
11. Bogner, W., Kramer, M., Krutzsch, B., Pishinger, S., Voigtlander, D., Wenninger, G., Wirbeleit, F., Brogan, M. S., Brisley, R. J., and Webster, D. E., *Appl. Catal. B: Environ.* **7**, 153 (1995).
12. Fridell, E., Skoglundh, M., Westerberg, B., Johanson, S., and Smedler, G., *J. Catal.* **183**, 196 (1999).
13. Mahzoul, H., Brilhac, J. F., and Gilot, P., *Appl. Catal. B: Environ.* **20**, 47 (1999).
14. Staff report, Modern Power Systems, March 2000.
15. U.S. Patent 5451558, 1995; U.S. Patent 5762885, 1998; U.S. Patent 5607650, 1997; U.S. Patent 5599758, 1997; U.S. Patent 5650127, 1997. [All of them assigned to Goal Line Environmental Tech.]
16. Nishino, T., Sakurai, T., Ishizawa, N., Mizutani, N., and Kato, M., *J. Solid State Chem.* **69**, 24 (1987).
17. Prinetto, F., Ghiotti, G., Nova, I., Lietti, L., Tronconi, E., and Forzatti, submitted.
18. Burch, R., Wathing, T. C., *Catal. Lett.* **43**, 19 (1997).